Staggering in γ-band energies and the transition between different structural symmetries in nuclei

E. A. McCutchan,[1,*] Dennis Bonatsos,[2,†] N. V. Zamfir,[3,‡] and R. F. Casten[1,§]

[1]*Wright Nuclear Structure Laboratory, Yale University, New Haven, Connecticut 06520-8124, USA*

[2]*Institute of Nuclear Physics, National Center for Scientific Research "Demokritos," GR-15310 Aghia Paraskevi, Attiki, Greece*

[3]*National Institute of Physics and Nuclear Engineering, Bucharest-Magurele, Romania*

(Received 5 March 2007; revised manuscript received 7 May 2007; published 3 August 2007)

The experimental energy staggering in γ bands of rare earths and actinides exhibits three distinct patterns as a function of angular momentum that are typical of well-deformed structural benchmarks: γ-soft for nuclei situated between a vibrator and a deformed γ-soft structure, axially symmetric for those between a vibrator and a rigid rotor, and triaxial γ-rigid for nuclei between a vibrator and a rigid triaxial rotor. The three patterns are reproduced by appropriate special solutions of the Bohr Hamiltonian, as well as by interacting boson approximation calculations. A particular quantity called S(4), which is proportional to the displacement of the 3^+_γ level relative to the average of the 2^+_γ and 4^+_γ levels, can vary in magnitude and sign for different shapes and is found to give a good indication of structure and the evolution of structure. A sudden change in the γ-band staggering occurring between the vibrator and the axially symmetric rotor limits seems to be connected to the known presence of a first-order phase/shape transition in this region.

DOI: 10.1103/PhysRevC.76.024306 PACS number(s): 21.60.Ev, 21.60.Fw, 21.10.Re, 27.60.+j

I. INTRODUCTION

When atomic nuclei deviate from spherical shapes, a separation of body-fixed and laboratory-fixed (Euler angles) coordinates is appropriate. The body-fixed shape has traditionally been described in terms of the variables β and γ where the former specifies the ellipsoidal quadrupole deformation and the latter the degree of axial asymmetry. The importance of the γ degree of freedom in nuclei with static quadrupole deformation has been known for decades. It has been an essential element of geometric and algebraic collective models and is being taken into account more and more in microscopic theories based on the mean-field and residual interactions. In this article, we address the former macroscopic models and compare experimental results with collective model predictions for observables relating to energy levels sensitive to the γ dependence of the potential.

In terms of the geometric collective model, early work centered around three basic forms of the potential for the γ degree of freedom. An axially symmetric potential was considered by Bohr and Mottelson [1] using a harmonic oscillator potential with a minimum at $\gamma = 0^\circ$, yielding predictions for the axially symmetric deformed rotor. Deviations from axial symmetry have frequently been described by two distinct approaches. Wilets and Jean [2] incorporated a γ-independent potential (one completely flat in the γ degree of freedom) giving the well known γ-soft structure, whereas Davydov, Filippov, and Chaban [3,4] considered a harmonic oscillator potential with a minimum at finite values of γ to develop predictions for a rigid triaxial rotor.

To distinguish the above potentials empirically, a useful quantity that is often known experimentally or is easy to measure in new nuclei is the energy staggering in the quasi-γ band. This staggering has long been considered as a key signature [5] of the γ dependence of the potential because, being a differential quantity, it is a very sensitive measure of the energy spacing. For example, the energy levels of the γ band in a γ-independent potential cluster as $(2^+_\gamma), (3^+_\gamma, 4^+_\gamma), \ldots$ opposite to the rigid triaxial rotor $(2^+_\gamma, 3^+_\gamma), (4^+_\gamma, 5^+_\gamma), \ldots$ clustering pattern. The evolution of the γ-band staggering between the above two limits has been investigated in the $A \sim 100$–130 mass region (see, for example, Refs. [6,7]), as well as more globally in Ref. [5]. However, the models usually considered in this context—either of rigid triaxial or γ-soft type—do not exhaust the possibilities. A broader perspective reveals a more complete understanding of staggering and its relation to the underlying potential.

In this article, three categories of transitional regions are considered:

(i) The γ-soft region between the vibrator and a deformed γ-soft structure where the potential is γ independent. This corresponds to the U(5) to O(6) transition region in the language of the interacting boson approximation (IBA) [8]. This is the region containing the critical point symmetry E(5) [9], as well as where a second-order phase transition [10] occurs in the IBA between U(5) and O(6).

(ii) The axially γ-rigid region between the vibrator and the axially symmetric rotor, characterized by a harmonic oscillator in γ with the minimum in γ close to zero. This is the U(5) to SU(3) transition region of the IBA, in which a first-order phase transition occurs [10]. This is also the region that has been described by the critical point symmetry X(5) [11].

(iii) The triaxial γ-rigid region between the vibrator and the rigid triaxial rotator, characterized by fixed γ values

*elizabeth.ricard-mccutchan@yale.edu
†bonat@inp.demokritos.gr
‡zamfir@tandem.nipne.ro
§richard.casten@yale.edu

between 0° and 30°, which has no direct analog in the framework of IBA-1 [8].

In this article, we will show that the experimental energy staggering in the quasi-γ band for collective even-even nuclei exhibits three clearly distinct patterns as a function of angular momentum in these three regions. It is then examined to what extent these patterns are reproduced by several special solutions of the Bohr Hamiltonian, incorporating different forms for the potential in the γ degree of freedom, as well as by the IBA. Finally, we will show that the analysis of the staggering across an isotopic chain can be a direct and simple method for understanding the evolution of structure and also possibly provide an indicator for phase-transitional behavior.

The geometrical models we consider are based on the above-mentioned E(5) [9] and X(5) [11] special solutions of the Bohr Hamiltonian. In the E(5) case, the potential is independent of γ with $u(\beta,\gamma) = u(\beta)$, whereas in X(5) it has the form $u(\beta,\gamma) = u(\beta) + u(\gamma)$, with $u(\gamma)$ taken as a harmonic oscillator centered at $\gamma = 0°$. In both cases the simple ansatz of approximating $u(\beta)$ at the critical point by an infinite square-well potential is employed. Incorporating this potential in the Bohr Hamiltonian yields parameter-free (except for scale) predictions for both energies and electromagnetic transition strengths. The realization that such a simple approximation of the potential describes rather well the properties of several nuclei [12–15] has sparked renewed interest in additional simple models to describe a richer array of structures spanning from spherical to deformed shapes. Keeping with the spirit of X(5) and E(5), these models are either parameter-free variants of X(5)/E(5) or incorporate a potential with a single free parameter.

The number of these new geometrical models is quite large and the list continues to grow. Here we discuss only a subset. The infinite square-well potential can be replaced by a potential involving powers of $\beta(u(\beta) = \beta^{2n}/2$, where n is an integer) giving the so-called X(5)-β^{2n} models [16] and E(5)-β^{2n} models [17,18]. These describe structures that span from the vibrational-like region up to the X(5) and E(5) solutions with increasing values of n.

In the original X(5) solution, the separation of the β and γ variables is approximate. An exact separation of variables can be achieved by considering a potential of the form [2]

$$u(\beta,\gamma) = u(\beta) + \frac{u(\gamma)}{\beta^2}. \tag{1}$$

Taking the potential in the γ degree of freedom to be $u(\gamma) = (3c)^2\gamma^2/2$ and $u(\beta)$ to be either an infinite square well or a harmonic oscillator in β gives the exactly separable X(5) model [ES-X(5)] and the exactly separable X(5)-β^2 model [ES-X(5)-β^2] [19], respectively. The spectra of most deformed nuclei can be reproduced for c values ranging from 2 to 20.

Special solutions of the Bohr Hamiltonian that give predictions for triaxial structures include the Z(4) [20] and Z(5) [21] models. In both of them, an infinite square-well potential in the β degree of freedom is used: in Z(4) the γ degree of freedom is frozen to $\gamma = 30°$, and in Z(5) a harmonic oscillator potential in γ with a rigid minimum at $\gamma = 30°$ is used.

II. γ-BAND ENERGY STAGGERING PATTERNS AS A FUNCTION OF ANGULAR MOMENTUM

Odd-even staggering in γ bands will be studied using the quantity [5]

$$S(J) = \frac{\{E(J_\gamma^+) - E[(J-1)_\gamma^+]\} - \{E[(J-1)_\gamma^+] - E[(J-2)_\gamma^+]\}}{E(2_1^+)}, \tag{2}$$

which measures the displacement of the $(J-1)_\gamma^+$ level relative to the average of its neighbors, J_γ^+ and $(J-2)_\gamma^+$, normalized to the energy of the first excited state of the ground band, 2_1^+. Because $S(J)$ is of (discrete) derivative form, it is very sensitive to structural changes. Figure 1 shows the low-lying ground band and γ-band levels for a vibrator, an axially symmetric deformed rotor, a deformed γ-soft structure, and a rigid triaxial rotor along with the corresponding values for $S(4)$ and the trends in $S(J)$. Each of these limits can be discussed in terms of some basic overall predictions for $S(J)$. In both the vibrator and γ-soft limits, a similar clustering of the γ-band levels is predicted resulting in an oscillating behavior in $S(J)$ that is negative for even spin and positive for odd spin. The overall magnitude of $S(J)$ is larger in the γ-soft limit and increases gradually with spin compared with the vibrator predictions that are smaller in magnitude and constant. For a triaxial potential, the level clustering is opposite, again giving oscillatory values of $S(J)$ but with an opposite phase, namely positive for even spin and negative for odd spin. As a function of increasing spin, the $S(J)$ values increase rapidly. In the limit of an axially symmetric deformed rotor (harmonic oscillator with a minimum at $\gamma = 0°$), the $S(J)$ values are positive, small, and constant as a function of spin.

A. Experimental systematics

Analysis of the experimental staggering in different isotopic chains reveals several different patterns. We first categorize these based on the standard limits discussed above, then compare the observed systematics to the predictions of more flexible geometrical and algebraic models to describe a wider range of structures.

The Xe, Ba, and Ce isotopes are well-known examples [7,22,23] of the transition between vibrational and γ-soft structures and ^{134}Ba was the first example [12] found for E(5). The staggering for the Xe, Ba, and Ce isotopes, traditionally associated with a γ-independent potential, is given in Fig. 2. All of these nuclei show strong staggering, with negative $S(J)$ values at even J and positive values at odd J.

The heavy rare-earth nuclei ($N > 82$), however, are well established to display axially symmetric behavior. In addition, ^{150}Nd [14], ^{152}Sm [13], ^{154}Gd [25], and ^{156}Dy [26] have been proposed as good candidates for the X(5) critical point symmetry. The staggering for the Sm-Er isotopes is shown in Figs. 3(a)–3(e). For the sake of clarity, we separate the chains into a few distinct groups. Fig. 3(a) illustrates the staggering pattern for the more vibrational-like ($R_{4/2} < 2.8$) nuclei. These nuclei again show a staggering pattern where $S(J)$ is negative

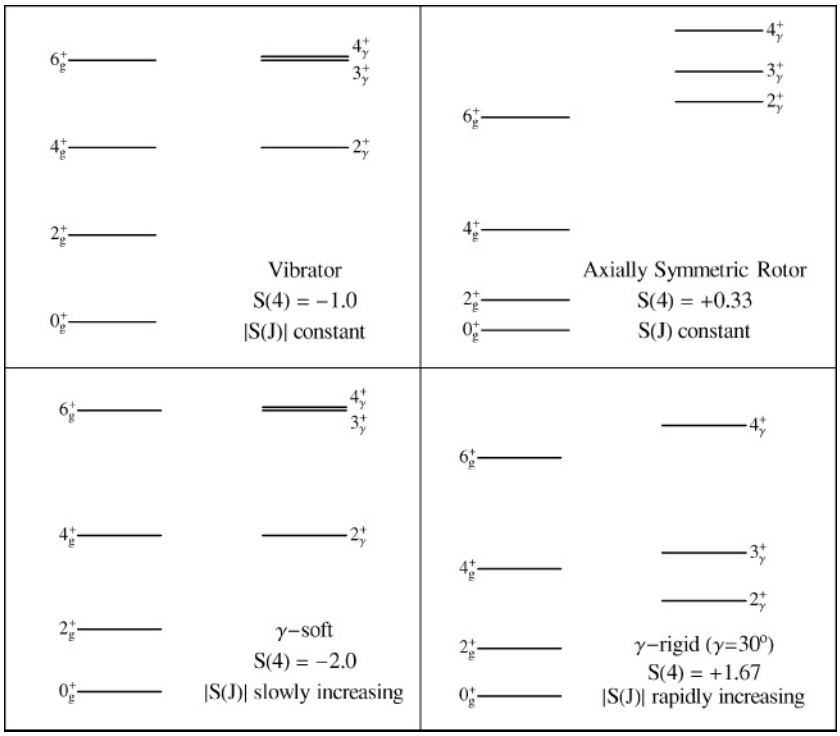

FIG. 1. Comparison of the energy spacings in the ground and γ band for a vibrator, axially symmetric rotor, γ-soft structure, and triaxial rotor. Included are the corresponding S(4) values and general trends in $S(J)$.

at even J values and positive for odd J values, with a smaller overall magnitude than that observed in the Xe, Ba, and Ce isotopes.

The staggering in the Sm and Gd isotopes is given in Fig. 3(b) and 3(c). The heavier Sm and Gd isotopes, ^{154}Sm and ^{158,160}Gd, exhibit more or less constant and very small values of $S(J)$, between $\sim$0.0 and 0.30. The nuclei ^{152}Sm and ^{154,156}Gd, however, each show a much more pronounced oscillatory pattern in $S(J)$. Still, comparison with the Xe, Ba, and Ce isotopes shows that the overall magnitude is much smaller.

Figures 3(d) and 3(e) give the staggering in the Dy and Er isotopes, respectively. For lower J values ($J \leqslant 7$), the staggering is small and more or less constant, with $S(J)$ ranging from $\sim$0.1 to 0.3. For some of these isotopes, ^{160,162}Dy and ^{162,164}Er, the staggering begins to grow larger for higher spin states ($J \geqslant 8$) and takes on a more pronounced oscillatory behavior. For completeness, the staggering for a few actinides where data are available is given in Fig. 3(f). These nuclei display very little change in $S(J)$ with increasing spin, with $S(J)$ values remaining constant around $+0.3$.

Nuclei that display staggering patterns very different from those described above are scarce but include ^{112}Ru, ^{170}Er, ^{192}Os, ^{192}Pt, and ^{232}Th, as shown in Fig. 4. For $J > 5$, these nuclei develop a staggering pattern where $S(J)$ is positive for even J and negative for odd J values. We note that the above list does not constitute a complete survey of all experimental data for such patterns, but merely highlights some select nuclei where such behavior has been observed.

B. Geometrical models

We now turn to the predictions of the geometrical models to determine if the observed staggering patterns can indeed be associated with different forms of the potential in the γ degree of freedom. Predictions from several geometrical models are summarized in Fig. 5. These fall into the three distinct categories given in the introduction. Figure 5(a) gives the staggering for those models that utilize a γ-independent potential. These models predict strong staggering with negative $S(J)$ values at even J and positive values at odd J. The absolute values of $S(J)$ increase when going from the vibrator limit to the γ-soft limit. In between one finds the critical point symmetry E(5), as well as the E(5)-β^{2n} models ($n = 2, 4$). The E(5)-β^2 model coincides with the vibrational limit.

It is clear that the staggering observed in the Xe, Ba, and Ce nuclei closely resembles the staggering pattern for a γ-independent potential found in Fig. 5(a). In some cases, the overall magnitude observed in the data is similar to the geometrical model predictions, as in the Ba isotopes, Fig. 2(b). For the Xe and Ce isotopes, however, the absolute values of $S(J)$ are slightly smaller than the model predictions.

Figure 5(b) shows those models that incorporate rigid triaxiality in the γ degree of freedom. Strong staggering is observed but with the opposite phasing, namely positive values for even J and negative values for odd J. The magnitude of the staggering is also larger, by about a factor of 2, than what is observed for the γ-independent potential. The staggering is largest for the Davydov model where it increases linearly with J. It is smallest for the Z(5)-β^2 and Z(4)-β^2 models, in which a harmonic oscillator β^2 potential is used instead of the infinite square-well potential. Intermediate lie the predictions of the Z(4) and Z(5) models. The staggering pattern observed in all the models in Fig. 5(b) is a hallmark for triaxiality [3].

Isolated cases of possible empirical triaxial behavior can be seen in Fig. 4. For $J > 5$, these nuclei begin to exhibit a staggering pattern similar to that of the triaxial

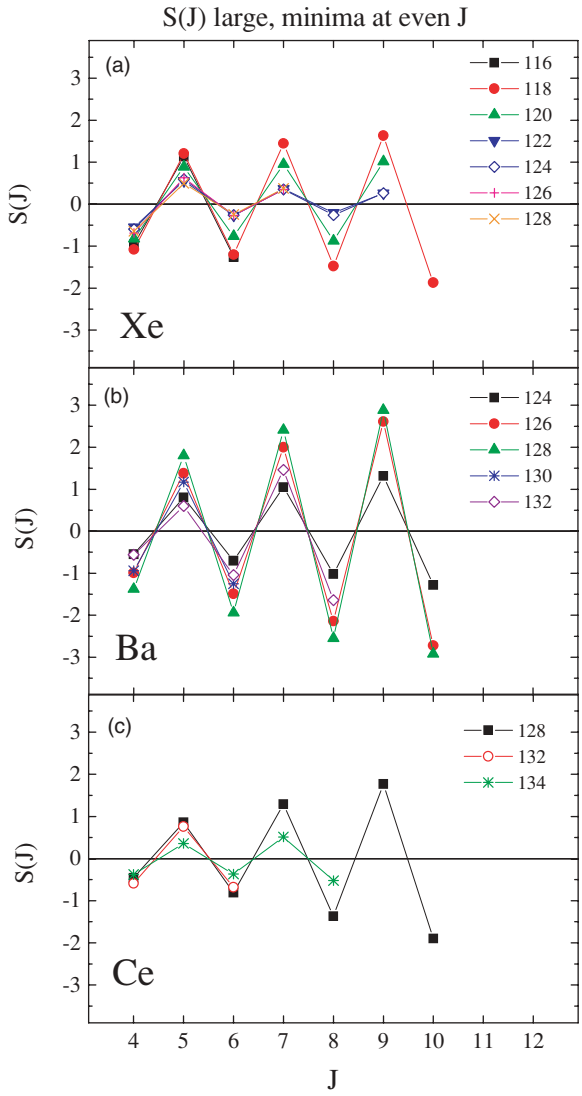

FIG. 2. (Color online) Experimental $S(J)$ [Eq. (2)] for several (a) Xe, (b) Ba, and (c) Ce isotopes. Data were taken from Ref. [24].

model predictions, although the overall magnitudes are much smaller.

Finally, in Fig. 5(c), several models that use a harmonic oscillator in the γ degree of freedom with minimum at $\gamma = 0^\circ$ are given. These models exhibit a very different behavior: the staggering does not show an oscillatory pattern but has only positive values of $S(J)$ for all spin values. These values are also much smaller than the previous model predictions shown in Figs. 5(a) and 5(b). The inset to Fig. 5(c) illustrates the staggering pattern if the same scale as Fig. 5(a) were used. The smallest values of $S(J)$ are seen in the X(5)-β^2 model. With increasing powers of β, the $S(J)$ values increase, reaching a value of $\sim$0.15 for the X(5) solution. The solutions ES-X(5) and ES-X(5)-β^2 lie in between the X(5) predictions and the rigid rotor value of 0.33. Also, there is only a small dependence on the parameter c, which is a measure of the stiffness of the potential in γ. For example, in the case of ES-X(5)-β^2, values of the parameter c of 5.0 and 15.0 give S(4) values of 0.21 and 0.23, respectively. To provide some feeling for how the magnitude of c varies the stiffness of the potential, the above example corresponds to $E(2^+_\gamma)/E(2^+_1)$ ratios of 6.8 and 19.2, respectively.

Perhaps the best examples of the behavior seen in Fig. 5(c) correspond to the actinide region. The staggering patterns observed in the actinides, Fig. 3(f), most closely resemble the predictions for an axially symmetric potential. The deformed Dy and Er isotopes also exhibit staggering patterns similar to what is expected for an axially symmetric potential, particularly at lower J values ($J \leqslant 7$). In the case of ^{160,162}Dy and ^{162,164}Er, the staggering resembles an axially symmetric potential at low spin, then appears to change to vibrational-like for higher spin states ($J \geqslant 8$).

The oscillatory pattern in $S(J)$ observed in ^{152}Sm and ^{154,156}Gd at first appears inconsistent with the axially symmetric model predictions given in Fig. 5(c). An oscillatory pattern in $S(J)$, similar to the one seen in ^{152}Sm and ^{154,156}Gd, however, can be obtained in the exact numerical diagonalization of the Bohr Hamiltonian with an infinite square well potential in β and a harmonic oscillator potential in γ provided by Caprio [27] for a parameter value that yields results which resemble the predictions of X(5), of which ^{152}Sm and ^{154}Gd are known to be good examples. For example, for a parameter value of $a = 200$ (where a is again a measure of the stiffness of the potential in γ and related to the parameter c by $c = \frac{\sqrt{a}}{3}$), the exact numerical diagonalization yields S(4), S(5), and S(6) values of -0.16, $+0.46$, and -0.31, respectively. These are very similar to the $S(J)$ values observed in ^{152}Sm.

C. Interacting boson approximation model

The idealized geometrical models discussed thus far provide a reasonable qualitative classification of the staggering patterns in the nuclei outlined above. We now consider the predictions of a more flexible model incorporating a few free parameters that can span a variety of structures continuously. Here we use the IBA model where calculations are performed using the usual two-parameter IBA-1 Hamiltonian [28,29]

$$H(\zeta, \chi) = C\left[(1-\zeta)\hat{n}_d - \frac{\zeta}{4N_B}\hat{Q}^\chi \cdot \hat{Q}^\chi\right], \qquad (3)$$

where $\hat{n}_d = d^\dagger \cdot \tilde{d}$, $\hat{Q}^\chi = (s^\dagger \tilde{d} + d^\dagger s) + \chi(d^\dagger \tilde{d})^{(2)}$, N_B is the number of valence bosons, and C is a scaling factor. The above Hamiltonian contains two parameters, ζ and χ, with the parameter ζ ranging from 0 to 1, and the parameter χ ranging from 0 to $-\sqrt{7}/2 = -1.32$. The three benchmarks of structure, harmonic vibrator, deformed axially symmetric rotor and γ-soft shapes correspond to the IBA dynamical symmetries U(5), SU(3), and O(6), respectively. In this parametrization, the IBA dynamical symmetries are given by $\zeta = 0$, any χ for U(5), $\zeta = 1$, $\chi = -\sqrt{7}/2$ for SU(3) and $\zeta = 1$, $\chi = 0$ for O(6). With this form of the IBA Hamiltonian, the minimum in the potential is always at $\gamma = 0^\circ$. The depth and sharpness of the potential is largest for $\chi = -\sqrt{7}/2$, gradually decreasing as $|\chi|$ decreases until $\chi = 0$, where the potential becomes totally independent of γ.

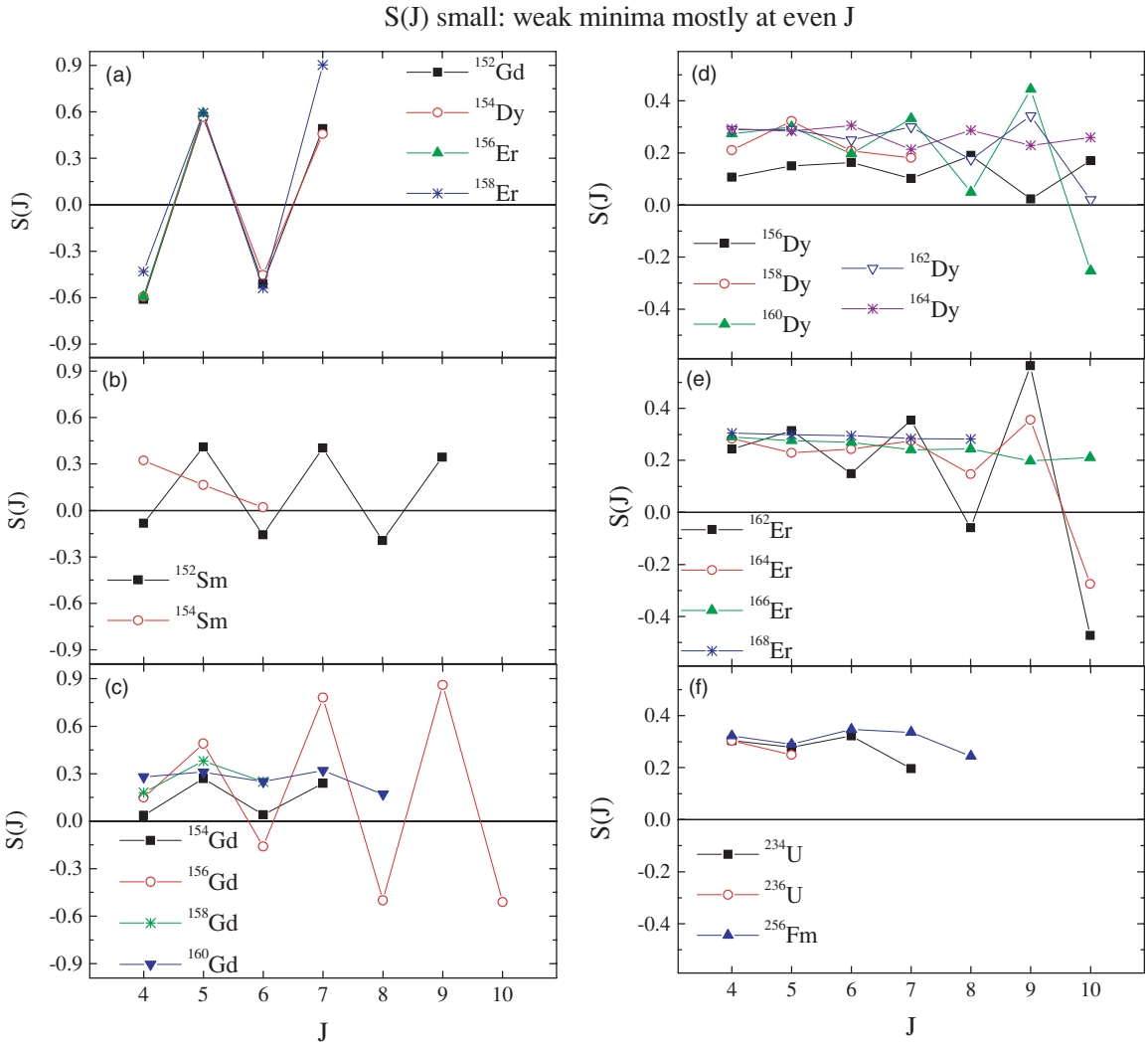

FIG. 3. (Color online) Experimental $S(J)$ [Eq. (2)] for (a) some vibrational rare-earth nuclei, (b) Sm, (c) Gd, (d) Dy, (e) Er, and (f) U and Fm isotopes. Data were taken from Ref. [24].

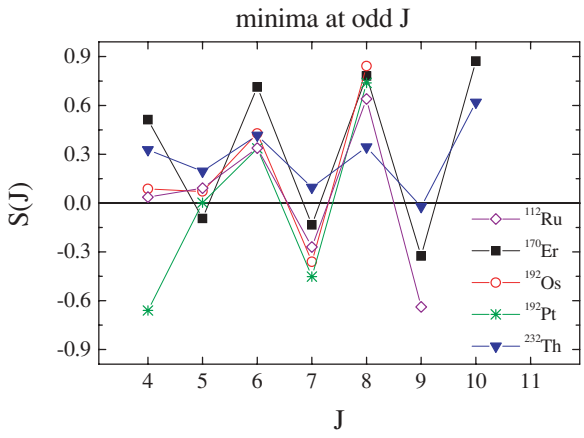

FIG. 4. (Color online) Experimental $S(J)$ [Eq. (2)] for ^{112}Ru, ^{170}Er, ^{192}Os, ^{192}Pt, and ^{232}Th that shows the staggering associated with triaxial shapes. Data were taken from Ref. [24].

We comment briefly on how the 2^+_γ state is assigned in the IBA calculations. Determining the state that corresponds to the γ band along two legs of the symmetry triangle [30] of the IBA, U(5) to O(6) and SU(3) to O(6), is straightforward because in both cases the γ band lies below the 2^+ member of the excited 0^+ sequence [except in SU(3) where the two are degenerate]. Identification of the 2^+_γ state along the U(5)-SU(3) transition is somewhat more challenging because the excited 2^+ states switch character along the transition. In the present analysis, we assign the 2^+_γ state based on the quadrupole moment. For example, for $N_B = 10$ and a ζ value of 0.40, the quadrupole moments of the first three 2^+ states are $Q(2^+_1) = -4.1$, $Q(2^+_2) = +1.5$, and $Q(2^+_3) = -3.2$. For a deformed nucleus, the spectroscopic quadrupole moment of the γ band has the opposite sign as those for $K = 0$ bands, suggesting that the 2^+_2 level corresponds to the 2^+_γ level. This is confirmed by the band structure that is clear from a conventional assignment according to the $B(E2)$ values. The situation is also clear for large ζ values where 2^+_3 is assigned as 2^+_γ because the corresponding quadrupole moment

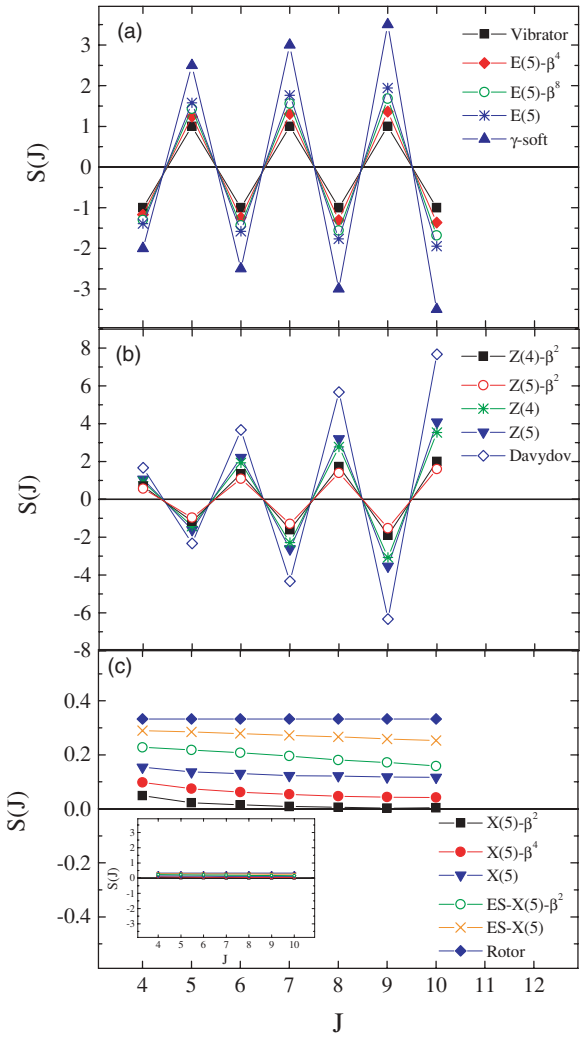

FIG. 5. (Color online) (a) Staggering $S(J)$ [Eq. (2)] for the vibrator and γ-soft limits, the E(5) critical point symmetry [9], and the E(5)-β^{2n} ($n = 2, 4$) models [17,18]. (b) Same for the Davydov model [3], the Z(5) [21] and Z(4) [20] models, as well as for their analogs Z(5)-β^2 and Z(4)-β^2. (c) Same for the axially symmetric rotor limit, the X(5) critical point symmetry [11], the X(5)-β^{2n} ($n = 1, 2$) models [16], and the exactly separable models ES-X(5)-β^2 ($c = 15$) and ES-X(5) ($c = 10$) [19], where the parameter c is related to the stiffness of the γ potential [$V(\gamma) = (3c)^2\gamma^2/2$].

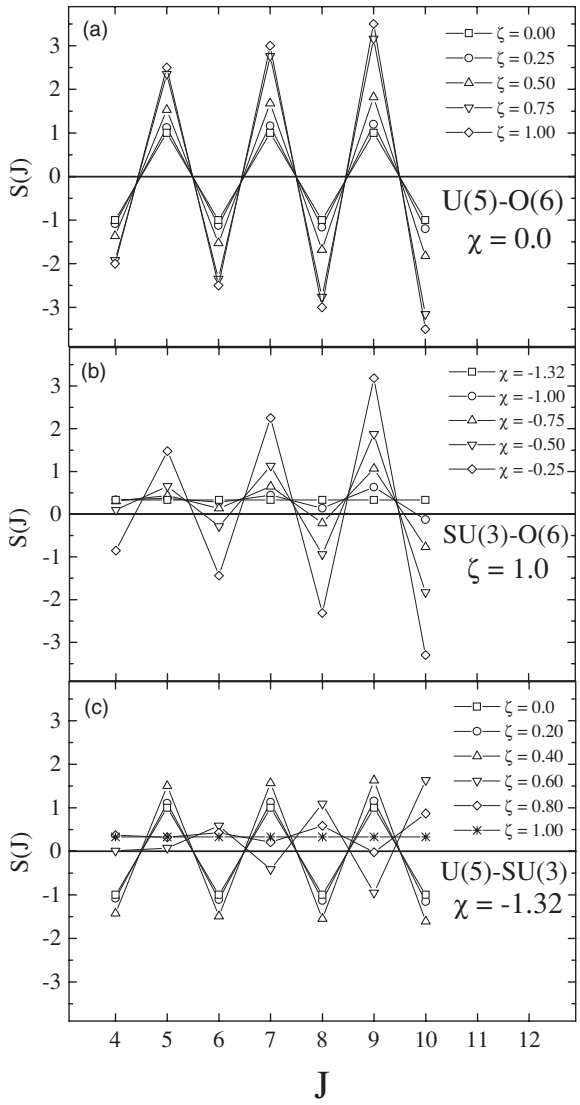

FIG. 6. Staggering $S(J)$ [Eq. (2)] from IBA [8] calculations with the Hamiltonian of Eq. (3). Included are calculations for (a) the U(5)–O(6) transition, (b) the SU(3)–O(6) transition, and (c) the U(5)–SU(3) transition. Calculations are for 10 bosons.

is positive. For example, for $\zeta = 0.60$ the quadrupole moments are $Q(2_1^+) = -7.2$, $Q(2_2^+) = -4.4$, and $Q(2_3^+) = +4.1$ There is only a small range of ζ values ($\zeta \sim 0.5$) where the excited 2^+ states are significantly mixed and their assignment based on $B(E2)$ values is difficult. In this case, we again assign 2_γ^+ based on the sign of the quadrupole moment.

Results of IBA calculations using the Hamiltonian of Eq. (3) are seen in Fig. 6. For the transition from U(5) to O(6), corresponding to $\chi = 0$ and ζ varying from 0 to 1, an identical staggering pattern to the one observed in Fig. 5(a) is seen, consistent with a γ independent potential. Moving from U(5) to O(6), the magnitude of $S(J)$ increases, in agreement with the geometrical model predictions in Fig. 5(a). Along the transition from SU(3) to O(6), achieved for $\zeta = 1$ and χ varying between -1.32 and 0, a transition from the SU(3) behavior of Fig. 5(c) to the O(6) behavior of Fig. 5(a) is seen. For large $|\chi|$, the staggering is small and more or less positive. As $\chi \to 0$, the oscillatory pattern becomes more and more pronounced.

Along the transition from U(5) to SU(3), obtained with $\chi = -1.32$ and ζ varying from 0 to 1, a U(5) like behavior, similar to Fig. 5(a), is seen up to $\zeta \sim 0.4$, surprisingly jumping over to a triaxial-like behavior similar to Fig. 5(b) for $\zeta \sim 0.6$. For $\zeta > 0.8$, the behavior predicted by the IBA starts to again resemble the predictions of the axially symmetric geometrical models given in Fig. 5(c). The tendency of developing minima at odd J can potentially be detected in some of the rotational nuclei given in Fig. 3, as, for example, in ^{156,158,164}Dy and ^{166}Er, albeit with much smaller oscillations in $S(J)$ than given by the IBA, in addition to the already mentioned pronounced cases of ^{170}Er and ^{232}Th.

III. γ-BAND ENERGY STAGGERING, S(4), AS A FUNCTION OF COLLECTIVE EVOLUTION

Having discussed how $S(J)$ varies as a function *spin* for different structures, it is now useful to look at how a particular signature, S(4), varies as a function of *structure*. We shall now focus our attention on S(4) [Eq. (2)], the displacement of the 3^+_γ state relative to the average of its neighbors, 2^+_γ and 4^+_γ, normalized to the energy of the 2^+_1 state. We investigate how S(4) changes for different structures using the energy ratio $R_{4/2} \equiv E(4^+_1)/E(2^+_1)$ as a structural indicator where $R_{4/2} =$ 2.0, 2.5, 3.33 for a vibrator, deformed γ-soft structure, and axially symmetric rotor, respectively. In the standard symmetry limits of the IBA, S(4) acquires the values -1 for U(5), -2 for O(6), $+0.333$ for SU(3). The corresponding values for the geometrical models outlined in Sec. II B are essentially the same for the corresponding geometrical potentials. A survey of the experimental staggering, S(4), in the $Z = 28$–82 nuclei and the comparison with E(5) symmetry is performed in Ref. [31].

Results of IBA calculations with the Hamiltonian of Eq. (3) for S(4) are shown as a function of the $R_{4/2}$ ratio in Fig. 7. A smooth evolution from U(5) to O(6), as well as from O(6) to SU(3), is seen. In the U(5) to SU(3) case, a sudden jump from large negative values in the vibrational limit to values close to zero occurs around $R_{4/2} \sim 2.5$. This sharp change is associated with a changing structure of the excited 2^+ states in the IBA. As discussed previously, for small $R_{4/2}$ values, 2^+_2 can be associated with the quasi-γ band, whereas 2^+_3 is a member of the excited 0^+_2 sequence. Beyond an $R_{4/2}$ value of 2.5, the assignment of these two states reverses.

A more systematic IBA study of S(4) vs. $R_{4/2}$ for different values of χ is seen in Fig. 8. S(4) evolves smoothly for values of χ down to -1, whereas a sudden jump to positive values is obtained for $\chi = -1.15$ and $\chi = -1.32$ [close to the U(5)-SU(3) leg of the symmetry triangle]. This rapid change in S(4) occurs roughly in the region of $R_{4/2}$ values between 2.4 and 2.6, which are the values corresponding to the X(3) [32] and X(5)-β^2 [16] models, found [33] to correspond to the left and right border of the phase/shape transition region near the U(5)-SU(3) leg of the IBA symmetry triangle. This suggests that the sudden change in S(4) may be related to the first-order phase/shape transition occurring between U(5) and SU(3): that is, for intermediate $R_{4/2}$ values between $\sim$2.2 and 3.1 the only region where S(4) is predicted to be near zero is very close to the phase/shape transition region in the IBA.

We return now to the predictions for S(4) in the different geometrical models, looking at the results as a function of $R_{4/2}$, as shown in Fig. 9. The geometrical models that incorporate a γ-independent potential, given in Fig. 9(a), show the same linearly decreasing behavior as the IBA calculations moving along the U(5)-O(6) leg of the symmetry triangle of the IBA [Fig. 7(a)].

The triaxial models, given in Fig. 9(b), do not resemble any of the results from the IBA calculations, evolving to larger and larger positive S(4) values with increasing $R_{4/2}$.

The models plotted in Fig. 9(c), involving a harmonic oscillator potential in γ with a minimum at $\gamma = 0^\circ$, show some similarities with the U(5)-SU(3) transition. Note that these

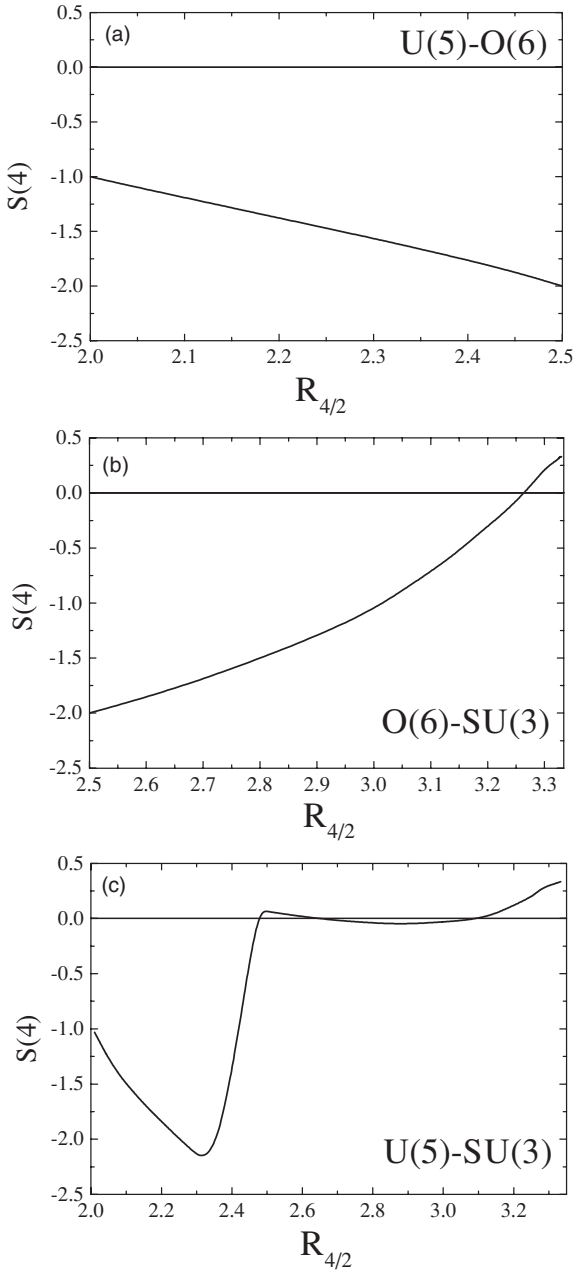

FIG. 7. Staggering S(4) [Eq. (2)] vs. $R_{4/2} = E(4^+_1)/E(2^+_1)$ from IBA [8] calculations with the Hamiltonian of Eq. (3) for (a) the U(5)–O(6) transition, (b) the O(6)–SU(3) transition, and (c) the U(5)–SU(3) transition. Calculations are for 10 bosons.

models start with predictions for a rather deformed structure ($R_{4/2} = 2.6$). The trend here is a growing S(4) value with increasing deformation, starting close to zero for $R_{4/2} \sim 2.6$ and increasing to the rigid rotor limit. However, all these S(4) values are very small.

We have seen that these models mirror, in general, the experimentally observed classes of nuclei. However, further insight can be obtained by considering to what extent the evolutionary patterns in S(4) versus $R_{4/2}$ given by the geometrical models and the IBA are realized in actual nuclei. The smooth evolution from U(5) (vibrator) to O(6) (γ-soft) seen in Figs. 7(a) and

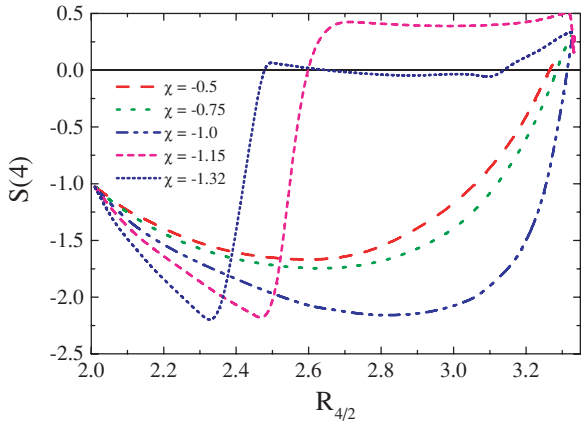

FIG. 8. (Color online) Staggering S(4) [Eq. (2)] for different values of the IBA parameter χ vs. $R_{4/2} = E(4_1^+)/E(2_1^+)$ from IBA [8] calculations with the Hamiltonian of Eq. (3). For each value of χ, the curve corresponds to varying the parameter ζ from 0 to 1. Calculations are for 10 bosons.

9(a), is manifested in the Xe and Ba isotopic chains shown in Fig. 10(a). Although the linear decreasing trend is similar, the overall magnitude of S(4) is observed to be less in the data compared with the predictions of both the geometrical models and the IBA.

The evolution from U(5) (vibrator) to SU(3) (axially symmetric rotor) seen in Figs. 7(c) and 9(c) corresponds to the Nd, Sm, Gd, Dy, and Er isotopic chains shown in Fig. 10(b). For each of these isotopic chains, S(4) always is small, consistent with the theory, and evolves from negative values for the more vibrational nuclei, passing close to zero for a single isotope along the chain and then increasing to the rigid rotor limit of 0.33. For example, the sudden jump in $R_{4/2}$ from 2.19 to 3.02 in ^{152,154}Gd and from 2.23 to 2.93 in ^{154,156}Dy occurs together with a sudden jump of S(4) from low negative to slightly positive values. It is clear that on the way from U(5) [S(4)= −1] to SU(3) [S(4) = +0.333], S(4) has to change sign. The data shown in Table I indicates that this change occurs in the neighborhood of the $N = 90$ isotones ^{150}Nd, ^{152}Sm, ^{154}Gd, and ^{156}Dy, which are known to be good examples [13,14,25,26] of the X(5) critical point symmetry. Thus, along the transition from vibrator to deformed axially

TABLE I. Experimental [24] energy ratios $R_{4/2} = E(4_1^+)/E(2_1^+)$ and staggering S(4) [Eq. (2)] for $N = 90$ isotones that are good examples [13,14,25,26] of the critical point symmetry X(5) [11] and their relevant neighbors, exhibiting a change of the sign of S(4) at the critical nucleus.

	$R_{4/2}$	$S(4)$
^{148}Nd	2.493	−0.301
^{150}Nd	2.929	+0.108
^{152}Sm	3.009	−0.081
^{154}Sm	3.254	+0.322
^{152}Gd	2.194	−0.605
^{154}Gd	3.015	+0.036
^{154}Dy	2.233	−0.594
^{156}Dy	2.934	+0.107

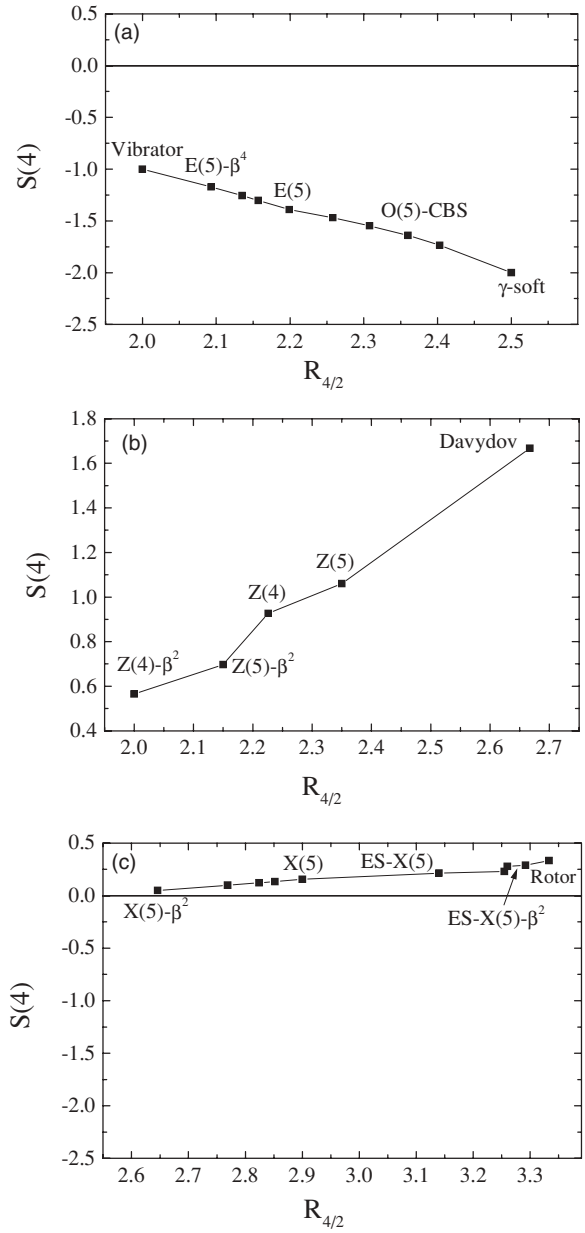

FIG. 9. (a) Staggering S(4) [Eq. (2)] vs. $R_{4/2} = E(4_1^+)/E(2_1^+)$ for the vibrator, the E(5) critical point symmetry [9], the E(5)-β^{2n} ($n = 2, 3, 4$) models [17,18], as well as for the O(5)-CBS model [34] with parameter values $r_\beta = 0.15$, 0.20, 0.25, and 0.30 and a γ-soft structure. (b) Same for the Davydov model [3], the Z(5) [21] and Z(4) [20] models, as well as for their analogs Z(5)-β^2 and Z(4)-β^2. (c) Same for the axially symmetric rotor, the X(5) critical point symmetry [11], the X(5)-β^{2n} ($n = 1, 2, 3, 4$) models [16], and the exactly separable models ES-X(5) and ES-X(5)-β^2 [19] for different values of the parameter c (5.0 and 15.0, 5.0, and 10.0, respectively), related to the stiffness of the γ potential ($V(\gamma) = (3c)^2\gamma^2/2$).

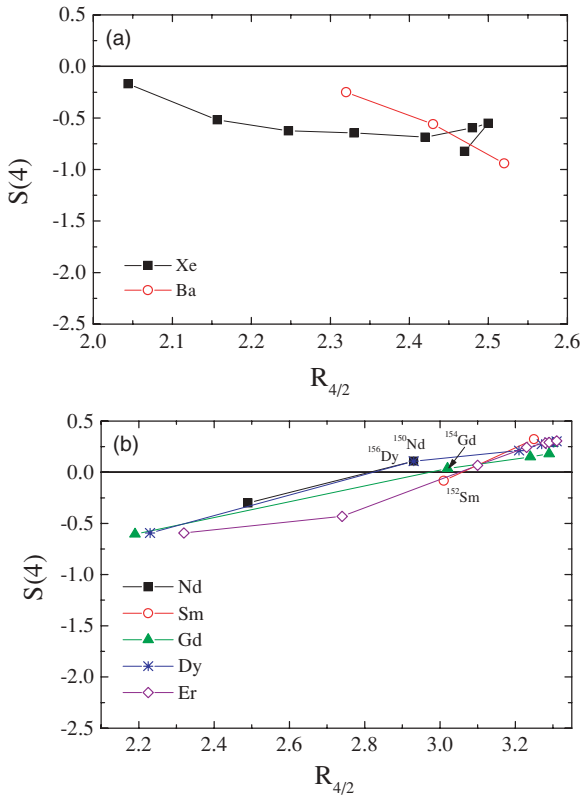

FIG. 10. (Color online) Experimental staggering S(4) [Eq. (2)] vs. $R_{4/2} = E(4_1^+)/E(2_1^+)$ for (a) Xe and Ba isotopes, including $^{120-134}$Xe and $^{130-134}$Ba and (b) for Nd, Sm, Gd, Dy, and Er isotopes, including ^{148,150}Nd, ^{152,154}Sm, $^{152-160}$Gd, $^{154-166}$Dy, and $^{156-168}$Er. Data have been taken from Ref. [24].

symmetric rotor, S(4) passing through or close to zero could be an indicator of a phase-transition region.

IV. CONCLUSION

In the present work, the experimental energy staggering in γ bands of several isotopic chains is investigated as a signature for the γ dependence of the geometric potential. Three distinct classes of energy staggering are found and discussed in terms of structure. Staggering patterns are first considered as a function of angular momentum. Strong staggering with minima at even spin is observed in the Ba, Ce, and Xe isotopes. The opposite behavior, strong staggering but with minima at odd spin is observed in a handful of select nuclei. Finally, the Sm-Er isotopes as well as the actinides are found to have staggering patterns much smaller in magnitude and for the most part rather constant in magnitude. Comparison with both geometrical model predictions and IBA calculations shows that the observed staggering patterns can be linked back to the underlying form of the potential in the γ degree of freedom.

The staggering quantity, S(4), is also investigated as a function of collectivity (using the $R_{4/2}$ ratio) along different isotopic chains. The Xe and Ba isotopes exhibit decreasing S(4) values as collectivity increases, similar in trend to both the geometrical model and IBA predictions with a γ-independent potential, but smaller in magnitude. In the Nd-Er isotopic chains, S(4) increases with increasing collectivity. This is consistent both in the trend and magnitude with the predictions of both the geometrical models and the IBA. Furthermore, the observed evolution of S(4) in the Nd-Er isotopic chains suggests that phase transitional behavior may occur close to where S(4) crosses zero.

ACKNOWLEDGMENTS

Work supported by U.S. DOE grant DE-FG02-91ER40609 and contract CEEX 05-D11-50 with the Romanian Authority for Scientific Research.

[1] A. Bohr and B. R. Mottelson, *Nuclear Structure: Nuclear Deformations* (World Scientific, Singapore, 1998), Vol. 2.
[2] L. Wilets and M. Jean, Phys. Rev. **102**, 788 (1956).
[3] A. S. Davydov and G. F. Filippov, Nucl. Phys. **8**, 237 (1958).
[4] A. S. Davydov and A. A. Chaban, Nucl. Phys. **20**, 499 (1960).
[5] N. V. Zamfir and R. F. Casten, Phys. Lett. **B260**, 265 (1991).
[6] J. Stachel, N. Kaffrell, E. Grosse, H. Elming, H. Folger, R. Kulessa, and D. Schwalm, Nucl. Phys. **A383**, 429 (1982).
[7] R. F Casten, P. von Brentano, K. Heyde, P. Van Isacker, and J. Jolie, Nucl. Phys. **A439**, 289 (1985).
[8] F. Iachello and A. Arima, *The Interacting Boson Model* (Cambridge University Press, Cambridge, 1987).
[9] F. Iachello, Phys. Rev. Lett. **85**, 3580 (2000).
[10] D. H. Feng, R. Gilmore, and S. R. Deans, Phys. Rev. C **23**, 1254 (1981).
[11] F. Iachello, Phys. Rev. Lett. **87**, 052502 (2001).
[12] R. F. Casten and N. V. Zamfir, Phys. Rev. Lett. **85**, 3584 (2000).
[13] R. F. Casten and N. V. Zamfir, Phys. Rev. Lett. **87**, 052503 (2001).
[14] R. Krücken *et al.*, Phys. Rev. Lett. **88**, 232501 (2002).
[15] A. Frank, C. E. Alonso, and J. M. Arias, Phys. Rev. C **65**, 014301 (2001).
[16] D. Bonatsos, D. Lenis, N. Minkov, P. P. Raychev, and P. A. Terziev, Phys. Rev. C **69**, 014302 (2004).
[17] J. M. Arias, C. E. Alonso, A. Vitturi, J. E. Garcia-Ramos, J. Dukelsky, and A. Frank, Phys. Rev. C **68**, 041302(R) (2003).
[18] D. Bonatsos, D. Lenis, N. Minkov, P. P. Raychev, and P. A. Terziev, Phys. Rev. C **69**, 044316 (2004).
[19] D. Bonatsos, D. Lenis, E. A. McCutchan, D. Petrellis, and I. Yigitoglu, Phys. Lett. **B649**, 394 (2007).
[20] D. Bonatsos, D. Lenis, D. Petrellis, P. A. Terziev, and I. Yigitoglu, Phys. Lett. **B621**, 102 (2005).
[21] D. Bonatsos, D. Lenis, D. Petrellis, and P. A. Terziev, Phys. Lett. **B588**, 172 (2004).
[22] G. Puddu, O. Scholten, and T. Otsuka, Nucl. Phys. **A348**, 109 (1980).
[23] R. F. Casten and P. von Brentano, Phys. Lett. **B152**, 22 (1985).
[24] Nucl. Data Sheets, through Vol. 106 (2005).

[25] D. Tonev, A. Dewald, T. Klug, P. Petkov, J. Jolie, A. Fitzler, O. Möller, S. Heinze, P. von Brentano, and R. F. Casten, Phys. Rev. C **69**, 034334 (2004).
[26] M. A. Caprio *et al*., Phys. Rev. C **66**, 054310 (2002).
[27] M. A. Caprio, Phys. Rev. C **72**, 054323 (2005).
[28] N. V. Zamfir, P. von Brentano, R. F. Casten, and J. Jolie, Phys. Rev. C **66**, 021304(R) (2002).
[29] V. Werner, P. von Brentano, R. F. Casten, and J. Jolie, Phys. Lett. **B527**, 55 (2002).
[30] R. F. Casten, *Nuclear Structure from a Simple Perspective* (Oxford University Press, Oxford, 1990).
[31] C. Mihai *et al*., Phys. Rev. C **75**, 044302 (2007).
[32] D. Bonatsos, D. Lenis, D. Petrellis, P. A. Terziev, and I. Yigitoglu, Phys. Lett. **B632**, 238 (2006).
[33] E. A. McCutchan, D. Bonatsos, and N. V. Zamfir, Phys. Rev. C **74**, 034306 (2006).
[34] D. Bonatsos, D. Lenis, N. Pietralla, and P. A. Terziev, Phys. Rev. C **74**, 044306 (2006).